Tulp3 quantitative alleles titrate requirements for viability, brain development, and kidney homeostasis but do not suppress *Zfp423* mutations in mice.

Corinne A. McCoy, Dorothy Concepcion, Mark G. Mezody, Raquel Z. Lara[†], Ojas Deshpande[†], Catherine Liang, Renee Long[†], and Bruce A. Hamilton

Department of Cellular and Molecular Medicine, Department of Medicine, Division of Genomics and Precision Medicine, Moores Cancer Center, and Institute for Genomic Medicine
UC San Diego School of Medicine, La Jolla, CA 92093

[†] Present addresses:
RL: Department of Dermatology, Stanford University School of Medicine, Redwood City, CA 94063
OD: University of Arizona College of Medicine, Phoenix, AZ 85004
RZL: University of Texas, Rio Grande Valley School of Medicine, Edinburg, TX 78541

ORCIDs:
CAM: 0000-0001-8960-414X
DC: 0000-0002-8506-1229
MGM: 0009-0009-0071-9852
RZL: 0000-0003-3769-9313
OD: 0000-0002-6029-2370
CL: 0009-0009-4808-514X
RL: 0000-0003-1638-3459
BAH: 0000-0001-5599-9139

ABSTRACT

Tubby-like protein 3 (TULP3) regulates receptor trafficking in primary cilia and antagonizes SHH signaling. *Tulp3* knockout mice are embryonic lethal with developmental abnormalities in multiple organs, while tissue-specific knockouts and viable missense alleles cause polycystic kidney disease. Human patients with *TULP3* mutations present with variable, but often multi-organ fibrotic disease. We previously showed that mouse and human *Tulp3* expression is negatively regulated by ZNF423, which is required for SHH sensitivity in some progenitor cell models. The level of TULP3 function required to prevent mutant phenotypes has not been known. Here we report a *Tulp3* quantitative allelic series, designed by targeting the polypyrimidine tract 5' to the splice acceptor of a critical exon, that shows distinct dose-response effects on viability, brain overgrowth, weight gain, and cystic kidney disease. We find limited evidence for genetic interaction with *Zfp423* null or hypomorphic mutations. Together, these results establish an approach to developing quantitative allelic series by exon exclusion, rank-order dose-sensitivity of *Tulp3* phenotypes, and model thresholds for TULP3 function to prevent severe outcomes.

Author Summary

TULP3 protein plays critical roles in regulating receptor trafficking and signaling in the primary cilium. Mutations in the *TULP3* gene can cause severe, multi-organ disorders in both mice and humans, yet the amount of *TULP3* activity needed to avoid these outcomes has been unclear. In this study, we used precise genome editing in mice to create a set of new *Tulp3* gene variants that reduce TULP3 expression to varying degrees. This allowed us to test how much TULP3 is required for survival, normal brain and kidney development, and weight regulation. We found that as little as 5% of normal *TULP3* levels is enough to avoid lethal birth defects, but still leads to obesity, mild brain overgrowth, and progressive kidney cysts preceded by reductions in cilium frequency and length in situ. The severity of these effects was related to TULP3 protein levels, highlighting a dose-dependent response. We also investigated whether reducing TULP3 levels would suppress brain abnormalities in *Zfp423* mutant mice, based on prior evidence of a genetic interaction, but did not find evidence to support this effect. Our work provides a framework for understanding how varying levels of *TULP3* affect various organ systems and offers a general strategy for creating quantitative genetic models of human disease.

57 **INTRODUCTION**

58

59 TUB-like protein 3 (TULP3), like TUB, is a phosphatidylinositol-(4,5)-bisphosphate (PIP2)
60 binding protein that is dynamically localized to different cell compartments, including plasma
61 membrane, nucleus, and primary cilia, during G protein coupled receptor signaling [1, 2]. TUB
62 and TULP3 are broadly expressed, close homologs [3] that promote trafficking of membrane
63 proteins into primary cilia through interactions with phosphatidylinositol-(4,5)-bisphosphate
64 (PIP2), the intraflagellar transport complex A (IFT-A), and cargoes–notably G protein-coupled
65 receptors and polycystins [4-10]. TULP3 antagonizes SHH signaling through its trafficking
66 activity [2, 4, 6, 11-13], with consequences for the development and function of several organ
67 systems. We previously showed that *Tulp3* is a target of *Zfp423* in both mouse and human cells
68 [14] and set out to test their genetic interaction *in situ*.

69

70 Mouse genetics identified functional requirements for *Tulp3* across several organs and cell
71 types. *Tulp3* mutants from either ES-cell targeting or chemical mutagenesis showed embryonic
72 lethality with exencephaly, spina bifida, preaxial polydactyly, splayed vertebrae, and increased
73 SHH activity [2, 12, 15]. A subsequent viable missense allele, *Tulp3*^{K407I} (a.k.a. *Tulp3*^{m1Kflj}), and
74 conditional deletion in either collecting ducts (*Tulp3*$^{tm1a(EUCOMM)Hmgu}$ with *Hoxb7*-Cre) or nephrons
75 (with *Ksp*-Cre) both showed polycystic kidneys in embryos or young mice, while simultaneous
76 deletions of *Tulp3* and the polycystin gene *Pkd1* suppressed the renal cysts seen in either
77 single gene deletion [16, 17]. Despite this progress, the amount of *Tulp3* function required for
78 viability and the dose-response for postnatal phenotypes have remained open questions and
79 direct comparisons across alleles in different labs are complicated by use of different genetic
80 backgrounds for each of these mutations.

81

82 Subsequent human studies identified biallelic damaging *TULP3* variants in patients with hepatic
83 fibrosis, fibrocystic kidneys, cardiomyopathy, and compromised DNA damage response [18],
84 which is a shared feature among several ciliopathy gene disorders [19-23]. Variants included
85 frameshift, nonsense, splice variant, and amino acid substitutions in the highly conserved TUB
86 domain. An additional patient reported later in ClinVar had a splice donor mutation after exon 7.
87 Onset and progression were variable among affected individuals in the documented cohort, but
88 liver and kidney damage preceded other organ involvement, with non-obstructive hypertrophic
89 cardiomyopathy reported only in a minority of patients and only in the sixth decade or later.
90 Typical for rare genetic disorders, how much of the variation in disease presentation is due to
91 allelic differences and how much to other causes–and how much functional recovery would be
92 required for benefit–are not known. Recent evidence has also implicated TULP3 in the effects of
93 caloric restriction on aging [24].
94
95 Given high levels of genetic heterogeneity (both locus and allelic) and variable penetrance of
96 disease phenotypes in human ciliopathies as well as differing genetic backgrounds and
97 individualized phenotyping protocols in animal models, relatively few studies have isolated
98 allele-specific effects from potential effects of genetic background and non-genetic factors.
99 Fewer have done so with quantitative alleles that titrate levels of genetic activity at the subject
100 locus. Here we develop a *Tulp3* quantitative allelic series in mice by editing the polypyrimidine
101 tract adjacent to a frame-shifting exon (exon 7) to modulate exon inclusion and expression level,
102 as well as qualitative variants lacking a conserved Tub-N domain (exon 4). We titrate clinically
103 relevant phenotypes across this series and test prior hypotheses for genetic interaction between
104 *Tulp3* and *Zfp423* mutations in mice. Our results establish a generalizable approach and show
105 that minimal (≤5%) of TULP3 expression level is required for viability, that modest increments of
106 expression improve clinically-related phenotypes, and that for at least one exon, loss of
107 conserved protein segments has a comparatively modest impact on genetic function.

108

109 **RESULTS**

110

111 **Quantitative allelic series by targeting inclusion of a frame-shifting exon.**

112 We targeted two sites in *Tulp3* based on its exon structure and protein coding domains, using a
113 high-fidelity Cas9 and a pool of donor oligonucleotides to template repair on a coisogenic
114 FVB/NJ genetic background (Figure 1A). We generated two mutations at exon 4, which
115 encodes a conserved protein domain, but whose skipping would maintain the open reading
116 frame in the resulting mRNA (Figure 1B). Both mutations should abolish exon 4 inclusion in
117 *Tulp3* mRNA but have residual genetic function unless the conserved Tub-N domain is essential
118 to all TULP3 activities. We targeted the polypyrimidine tract 5' to *Tulp3* exon 7 splice acceptor to
119 decrease the exon inclusion rate in processed mRNA. Exon 7 was selected based on its
120 exclusion resulting in a reading frame shift, such that the rate of exon 7 inclusion should predict
121 the degree of genetic function of an edited allele. We recovered seven distinct alleles from a
122 single injection job, including all four templated by the oligonucleotide pool and three
123 insertion/deletion (indel) variants, of which two (Δ5, Δ3) were predicted to abolish exon 7
124 inclusion and function as null mutations (Figure 1C). Oligonucleotide donors for editing and
125 assay primers are given in S1 and S2 Tables.

126

127 RT-PCR assays show that the exon 7 mutations result in reduced exon 7 utilization. Exon
128 inclusion assays showed inclusion rates that quantitatively distinguished alleles (Figure 1D).
129 The non-templated 4-bp insertion allele (i4) predicted a strong alternative splice acceptor that
130 would produce a frameshift without inducing exon skipping. DNA sequencing of the RT-PCR
131 product from an *i4* homozygote of steady-state *Tulp3* RNA is spliced into this upstream decoy
132 site rather than the in-frame splice acceptor (Figure 1E).

133

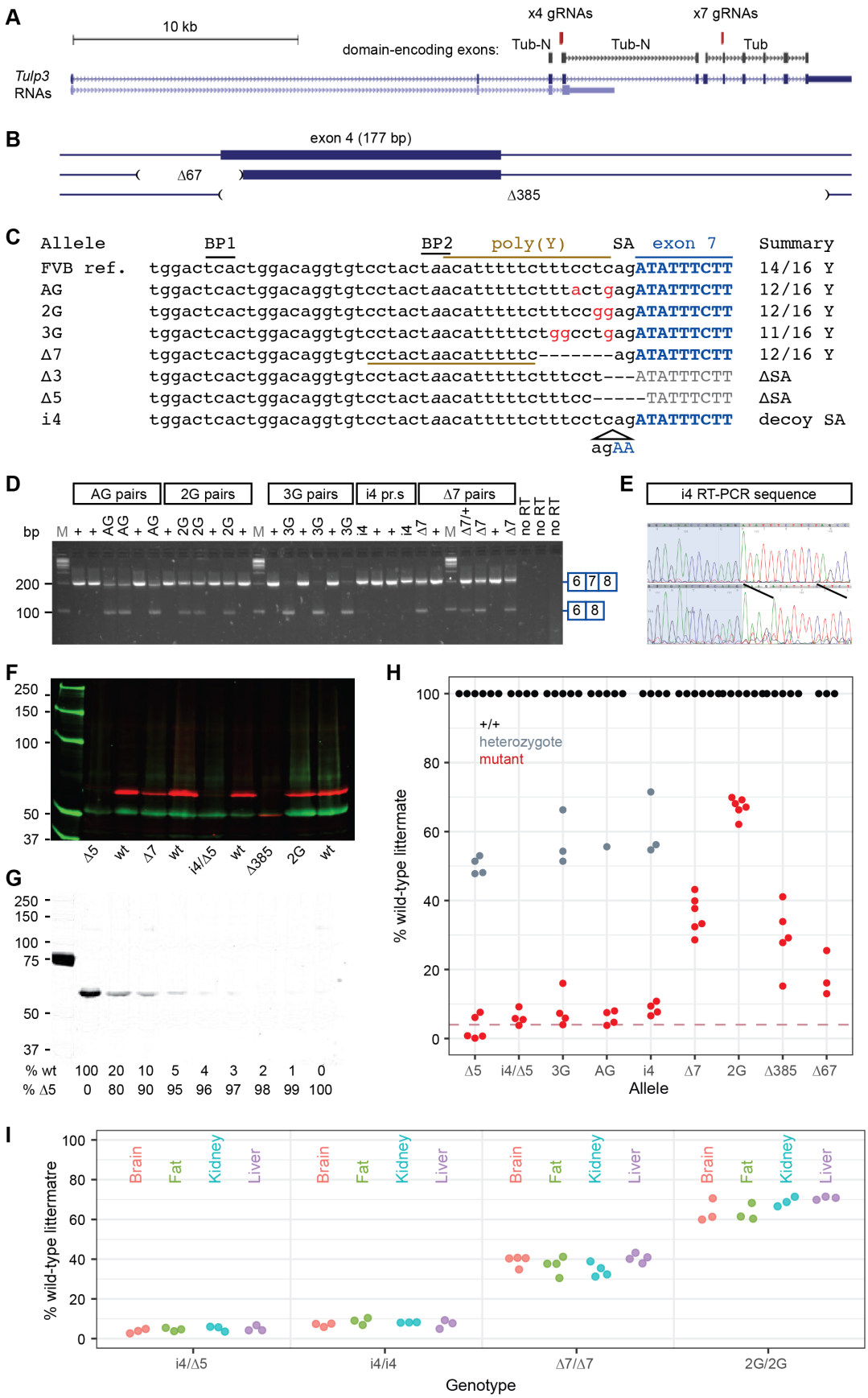
A
10 kb
x4 gRNAs
x7 gRNAs
domain-encoding exons:
Tub-N
Tub-N
Tub
Tulp3 RNAs
B
exon 4 (177 bp)
Δ67
Δ385
C
Allele BP1 BP2 poly(Y) SA exon 7 Summary
FVB ref. tggactcactggacaggtgtcctactaacatttttctttcctcagATATTTCTT 14/16 Y
AG tggactcactggacaggtgtcctactaacatttttctttactgagATATTTCTT 12/16 Y
2G tggactcactggacaggtgtcctactaacatttttctttccggagATATTTCTT 12/16 Y
3G tggactcactggacaggtgtcctactaacatttttctggcctgagATATTTCTT 11/16 Y
Δ7 tggactcactggacaggtgtcctactaacatttttc-------agATATTTCTT 12/16 Y
Δ3 tggactcactggacaggtgtcctactaacatttttctttcct---ATATTTCTT ΔSA
Δ5 tggactcactggacaggtgtcctactaacatttttctttcc-----TATTTCTT ΔSA
i4 tggactcactggacaggtgtcctactaacatttttctttcctcagATATTTCTT decoy SA
agAA
D
AG pairs
2G pairs
3G pairs
i4 pr.s
Δ7 pairs
bp
200
100
6 7 8
6 8
E
i4 RT-PCR sequence
F
250
150
100
50
37
Δ5 wt Δ7 wt i4/Δ5 wt Δ385 2G wt
G
250
150
100
75
50
37
% wt 100 20 10 5 4 3 2 1 0
% Δ5 0 80 90 95 96 97 98 99 100
H
+/+
heterozygote
mutant
% wild-type littermate
Δ5 i4/Δ5 3G AG i4 Δ7 2G Δ385 Δ67
Allele
I
Brain Fat Kidney Liver
% wild-type littermatre
i4/Δ5 i4/i4 Δ7/Δ7 2G/2G
Genotype

Figure 1. Allelic series targeting polypyrimidine tracts. (**A**) Genomic organization of *Tulp3* showing targeted exons relative to encoded domains. (**B**) Deletion alleles relative to exon 4. (**C**) Exon 7 alleles relative to FVB/NJ reference sequence. BP, splicing branch points; SA, splice acceptor; poly(Y), polypyrimidine tract. (**D**) RT-PCR shows allele-dependent levels of exon skipping induced by mutations in the polypyrimidine tract 5' to exon 7. (**E**) Sanger sequence of a control (top) and *i4* homozygote (bottom) shows a majority of steady-state RNA spliced into the mutant-specific decoy splice acceptor. (**F**) Two-color Western blot detects TULP3 (red, upper) and loading control (green, lower) from E14.5 heads relative to size marker (kD). (**G**) Null (Δ5/Δ5) protein extracts with wild-type spike-in estimates detection limit at ~4% of control. (**H**) Band intensities relative to littermate controls define a quantitative allelic series based on reduced TULP3 protein expression. Dashed line, 4%. (**I**) Band intensities relative to littermate controls for show do not find nominally significant differences across four tissues at P29 (p-values 0.11 to 0.56 for each genotype, one-factor ANOVA).

Western blots confirmed and quantified reductions in TULP3 protein expression across the allelic series. Extracts from E14.5 embryo littermate pairs showed reduced expression of otherwise wild-type TULP3 protein from each of the exon 7 alleles, with a reduced steady-state amount of a smaller TULP3 protein from the exon 4-skipping alleles (Figure 1F). Spike-in controls showed a detection limit at ~4% of wild-type levels under our conditions (Figure 1G). The very low levels achieved by splicing variants and null heterozygote expression at 50% suggest little to no compensatory feedback regulation for TULP3 levels. The lowest expression genotype, i4/Δ5 compound heterozygotes, expressed ≤5% of wild-type littermate TULP3 levels (Figure 1H and S3_Table). For viable genotypes, expression level did not vary significantly among four tissues relevant to *Tulp3* phenotypes at postnatal day 29 (Figure 1I and S4_Table). These results demonstrate simple construction of a quantitative allelic series that can be used for calibrating genetic function relative to *TULP3* phenotypes or potential interventions, using an approach that should be generalizable to other genes and across organ systems.

147

148 **Minimal TULP3 is required for survival to adulthood.**

149 Having a quantitative allelic series on a coisogenic background allowed us to estimate the
150 amount of *Tulp3* genetic function required to escape lethality and other major phenotypes. The
151 Δ5 splice acceptor mutation behaved as a genetic null. Homozygous Δ5 embryos produced no
152 detectable TULP3 protein and showed brain overgrowth resulting in exencephaly and preaxial
153 polydactyly resulting in supernumerary digits by E14.5 (Figure 2A), consistent with previous
154 knockout models on other strain backgrounds [2, 11, 12, 15]. Postnatally, we found no surviving
155 homozygotes among ~200 progeny from null-allele heterozygote crosses (Figure 2B). By
156 contrast, hypomorphic genotypes, including the i4/Δ5 allelic combination that expressed only
157 ~5% of normal TULP3 levels showed no significant evidence for reduced viability in moderately
158 large crosses. A nominal effect of the least severe allele, 2G, did not survive correction for
159 family-wise error rate and included the caveat that allele-specific PCR assays for 2G, 3G, and
160 AG were tuned to avoid homozygote false-positives and therefore likely under-count true
161 homozygotes. Pooling hypomorphic allele data from all length-specific assays (i4/Δ5, i4, Δ7, and
162 the two exon 4 deletions) was not significant despite large aggregate sample (p=0.17, Chi-
163 squared test). Littermate pairs selected for age-dependent phenotypes similarly failed to support
164 a significant effect of hypomorphic genotypes on later survival (likelihood ratio test p = 0.9 for
165 i4/Δ5, n = 29 littermate pairs to 150 days; p = 0.5 for combined pool of i4/Δ5, i4/i4, 3G/3G, and
166 AG/AG strong alleles, n = 84 littermate pairs; p = 0.5 for exon 4 deletion, n = 61 littermate pairs;
167 p = 0.2 for 248 littermate pairs across all variants). These results suggest that for severe *Tulp3*
168 phenotypes, even small increments of improved function might be beneficial, with only ~5% of
169 wild-type levels required for gestation and long-term survival.

A

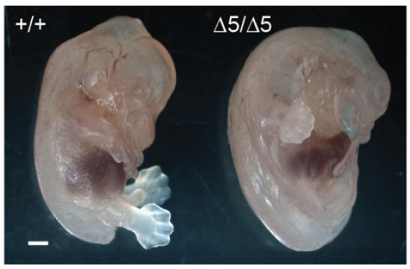

B

Allele	non-mut	mut	χ^2 p	FWER-adj p
Δ5	196	0	6.3×10^{-16}	6.3×10^{-15}
Δ3	134	0	2.3×10^{-11}	2.1×10^{-10}
i4/d5	228	69	0.48	0.92
3G	223	57	0.073	0.51
AG	263	73	0.17	0.75
i4	266	79	0.37	0.90
Δ7	113	34	0.60	0.92
2G	213	52	0.043	0.30
Δ67	358	105	0.25	0.80
Δ385	362	122	0.92	0.92

Figure 2. Minimal TULP3 expression is sufficient for viability and survival to adulthood. (**A**) Exencephaly and polydactyly are evident by E14.5 in Δ5 homozygotes. Bar, 1 mm. (**B**) Genotype ratios show complete lethality of null animals, but no significant evidence for reduced viability among even the strongest hypomorphic genotypes with TULP3 expression near the limit of detection in Western blots. Nominal p-values from the 1-df chi-squared test were adjusted for family-wise error rate (FWER-adj p) using Hommel's method [25].

170

171 **Hypomorphic *Tulp3* genotypes gain excess weight.**

172 From littermate pairs left during several months of the COVID-19 pandemic, *Tulp3* hypomorphic
173 mutants were visibly obese relative to co-housed same-sex littermates (Figure 3A and
174 S5_Table). As a more quantitative test and to determine the time course for onset, we followed
175 co-housed, same-sex littermate mutant-control pairs with periodic weight measurements in a
176 subsequent cohort from weaning to >6 months. For the lowest TULP3-expressing genotype
177 (i4/Δ5), a clear trend showed increasing weight gain over time by mutants relative to their
178 littermate controls for both sexes (Figure 3B). Results from other mutants showed similar though
179 less pronounced trends, roughly proportional to expression level and loss of exon 4 (Figure 3C).
180 As some littermate pairs were censored at later times due to age-related health issues
181 independent of genotype, we examined pairs weighed at 100-132 days postnatal (Figure 3D).
182 While modest sample sizes and corrections for family-wise error rate limited power for individual
183 genotypes, aggregating variants whose effect on TULP3 expression was relatively weak (2G,
184 Δ5/+, and Δ7), weak but included removal of exon 4 (Δ67, Δ385), or relatively strong (i4, AG,

185 3G) showed a rough correlation between weight gain and TULP3 expression loss. We saw
186 significant effects of all but the weak alleles, with exon 4 alleles roughly comparable to strong
187 alleles, and with the i4/Δ5 combination having a stronger effect than all others. These data show
188 a quantitative effect of TULP3 expression level on weight homeostasis at levels below 30% of
189 wild-type.

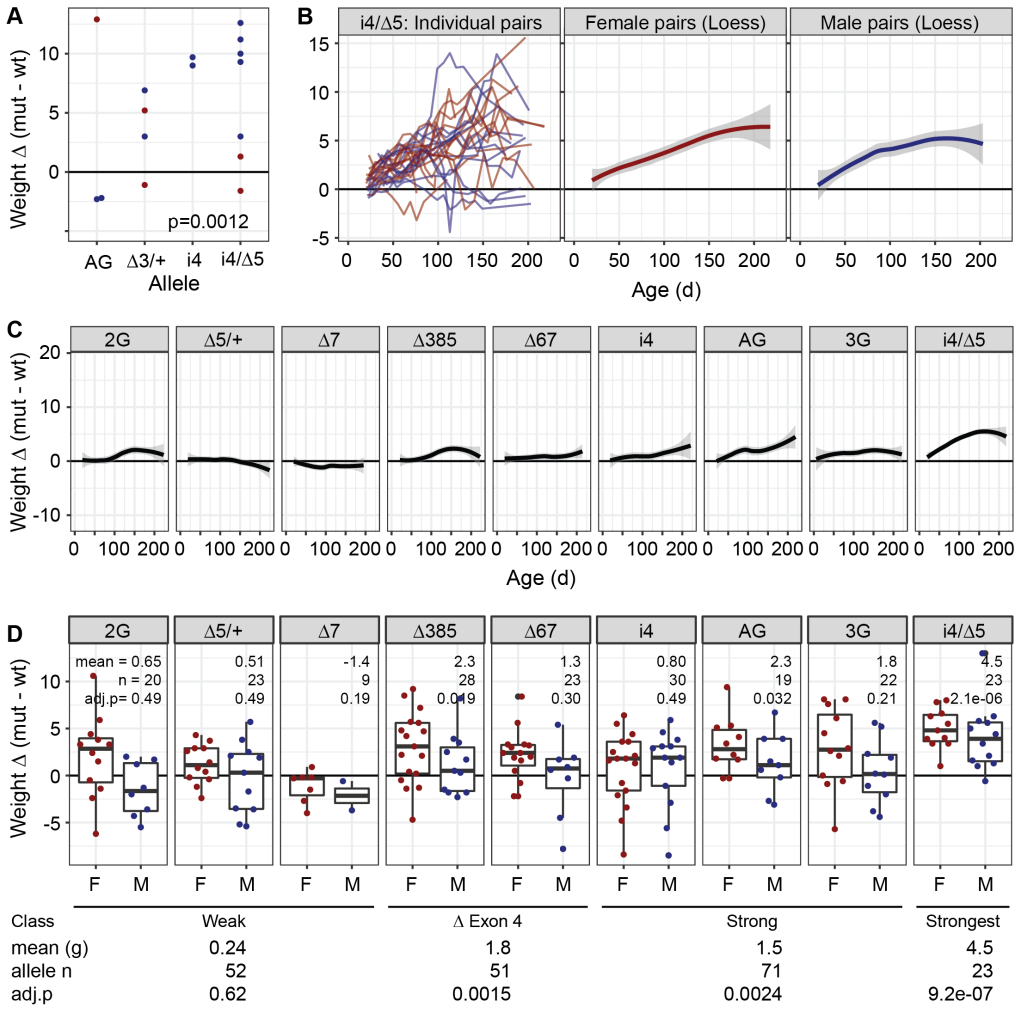

Figure 3. Allele-dependent weight gain in *Tulp3* hypomorphs. (**A**) Incidental observation of co-housed sex-matched littermates showed obesity in aged *Tulp3* mutants. Each point is the difference (mutant-wildtype) in grams for a littermate pair. Mean age 220 days. (**B**) Time course of weight difference in individual i4/Δ5 littermate pairs and loess regression plots of i4/Δ5 pairs for each sex. (**C**) Loess plots for each allele, both sexes. (**D**) Summary boxplots

with points for distinct individual pairs (first measure after postnatal day 100) for each *Tulp3* allele. Mean difference in grams, sample size, and FWER-corrected p-values from paired sample t-tests are given for each allele (above) and expression class (below).

Strongest reduction in *Tulp3* produces increases in brain measures.

Tulp3 knockout mice, including Δ5 allele homozygote reported here, display multisystem disorders including exencephaly secondary to brain overgrowth (Figure 4 and S6_Table). To determine whether viable *Tulp3*-mutant mice display related changes to gross brain morphology, we adopted a pipeline of 8 simple measures (vermis width, cerebellar hemisphere anterior-posterior distance, and maximum brain width from dorsal photographs of whole brain; vermis sagittal area, cortical thickness, corpus callosum thickness, and anterior commissure thickness from block face preparation photographs) that we previously used for analysis of *Zfp423* allelic variants [26]. We found that i4/Δ5 compound heterozygotes, the most severe viable genotype with respect to TULP3 protein level, had increased vermis sagittal area and cerebellar hemisphere anterior-posterior distance (4.5-6.0%) after correction for multiple outcome measures, with nominal support for increased brain width (2.6%), relative to same-sex littermate controls (Figure 4). Pooled data from the next most severe genotypes (i4/i4, AG/AG,

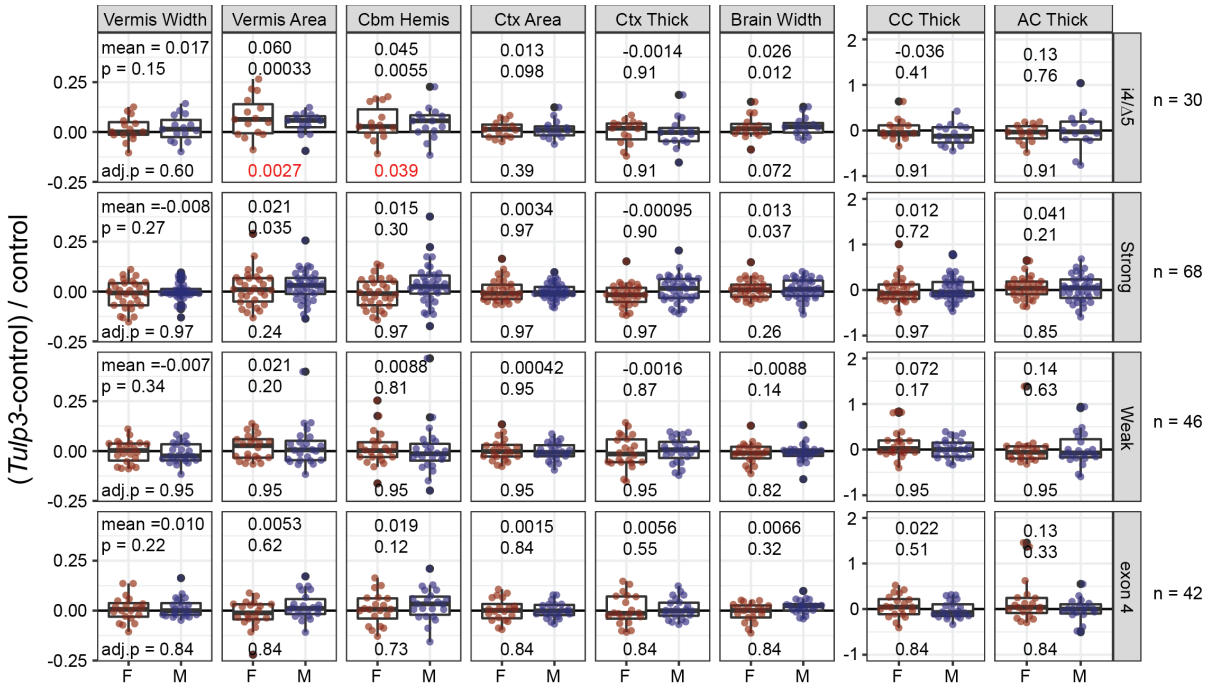

Figure 4. The strongest viable *Tulp3* variants influence brain morphology. (**A**) Compound heterozygotes i4/Δ5 average ~5-6% larger cerebellar vermis sagittal areas and anterior-posterior dimension of the cerebellar hemispheres. The widest extent of the brain was also nominally larger, but did not survive correction for multiple phenotypes (top row). Other strong hypomorphic genotypes (i4/i4, 3G/3G, AG/AG; combined to improve power across a similar expression level) showed nominal support for a lesser increase in vermis area and brain width that did not survive correction (second row). Neither the weaker exon 7 alleles (2G and Δ7) nor the exon 4 deletions (Δ67, Δ385) returned even nominally significant results for any measure. Mean, nominal p-value (paired sample t or Wilcoxon signed rank test), and adjusted p-value after FWER correction across 8 phenotype measures are shown. Abbreviations: Cbm Hemis, anterior-posterior dimension of the cerebellar hemispheres; Ctx Area, cortical area in dorsal surface view; Ctx Thick, average cortical thickness at 15°, 30°, and 45° from midline in coronal block face view; CC and AC Thick, thickness of the corpus callosum and anterior commissure, respectively, at the midline.

204 and 3G/3G) showed nominal increases in vermis area and brain width (1.3-2.1%) that did not
205 survive correction for multiple tests. These data show that even viable reduction in TULP3 can
206 result in modest brain overgrowth phenotypes and reinforce the conclusion that even modest
207 increases in *Tulp3* function can significantly impact phenotypic outcomes.
208
209 **Progressive kidney cystogenesis responds to small increments of TULP3 expression.**
210 *Tulp3* tissue-specific knockouts and a viable missense variant had cystic kidney disease, but
211 neither the time course of disease nor the quantitative level of gene function to reduce or
212 ameliorate primary endpoints have been known. We quantified a cystic index for sectioned
213 kidneys from same-sex littermate pairs across a range of ages for each *Tulp3* allele using
214 CystAnalyzer [27] (Figure 5 and S7_Table). The presence and size of cysts in aged animals
215 visibly varied across alleles (Figure 5A). Cysts were evident for each of the strong exon 7 alleles
216 but less frequent or not evident for weaker alleles that expressed ≥30% of control levels of
217 TULP3 (Figure 1G). The two exon 4 deletion/skipping alleles combined showed a reproducibly
218 low level of cysts, consistent with the relatively low steady-state protein level we observed, but
219 not consistent with exon 4 encoding an essential function. The extent of cystogenesis for each
220 genotype inversely correlated with expression level and increased with age (Figure 5B). In a
221 two-factor ANOVA model, genotype ($p = 7.5 \times 10^{-7}$) and age ($p = 0.043$) were significant, with
222 significant pairwise differences between i4/Δ5 and all others ($p < 1 \times 10^{-2}$), and between i4 and
223 3G ($p = 0.034$) or weaker alleles, but i4 and AG were not statistically different ($p > 0.99$). Cystic
224 index was both more sensitive and better correlated to TULP3 expression than simpler
225 measures of kidney weight relative to body weight or kidney cross-sectional area (Supplemental
226 S1_Figrue A-B). These data support a continuous relationship between kidney health and
227 TULP3 expression below 50%, with particularly steep dose-response effects below ~10% of
228 control levels.
229

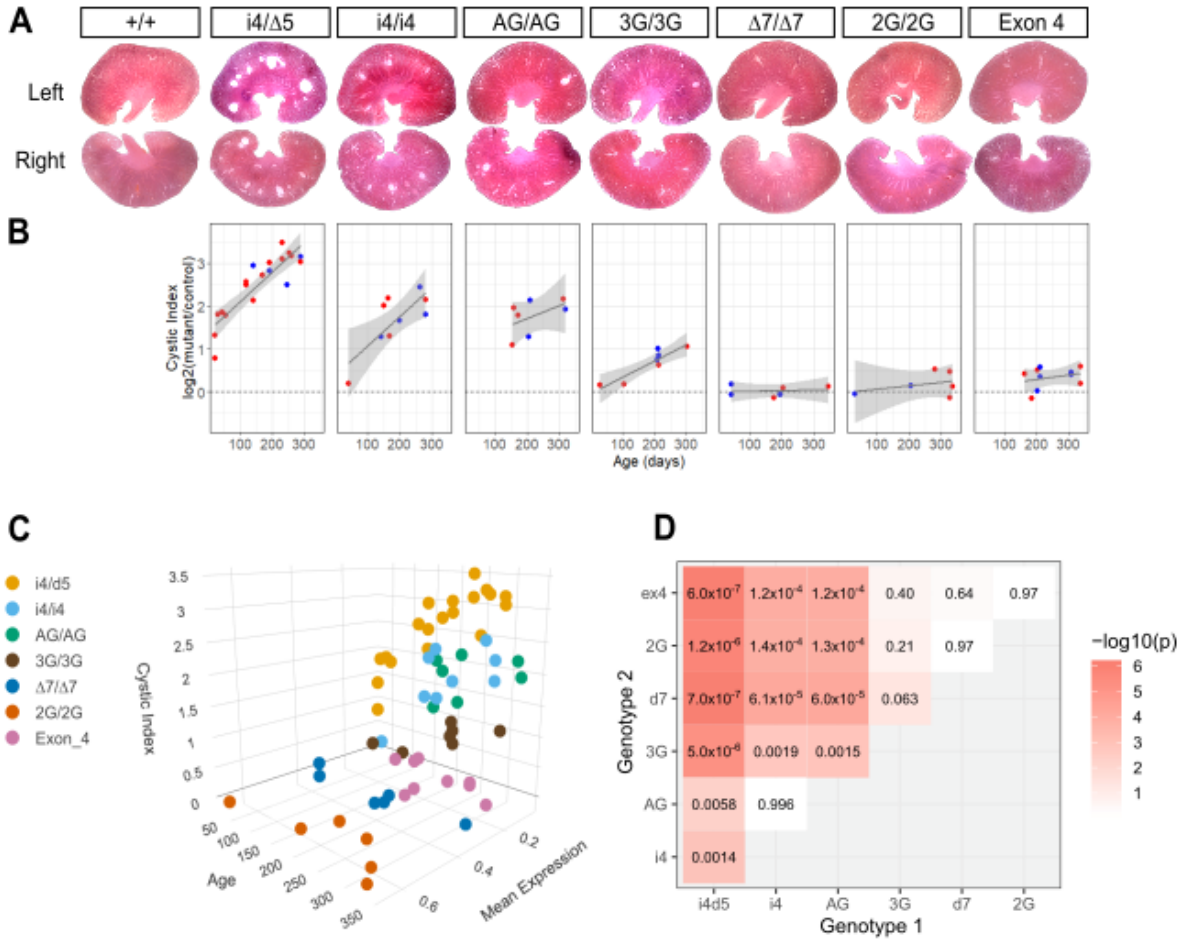

Figure 5. Allelic series shows dose-response in kidney cystogenesis. (**A**) Kidney sections from aged adult mice show allele-typical degrees of cystogenesis. (**B**) Cystic index for *Tulp3* variants showed allele- and age-dependence relative to same-sex control littermates. A generalized linear fit and 95% confidence interval are shown. (**C**) Three-dimensional visualization illustrates a sharp shift in cystic index across TULP3 expression levels. (**D**) Heatmap with printed values for TukeyHSD post-hoc test for difference between genotypes after two-factor ANOVA for cystic index as a function of genotype and age.

230 Despite evident tissue damage, veterinary blood chemistries from aged littermate pairs
231 (minimum 119 days, mean 234) did not detect differences in standard measures across 16
232 sample pairs from strong hypomorphic alleles (Supplemental Figure S1_Figure and S8_Table).

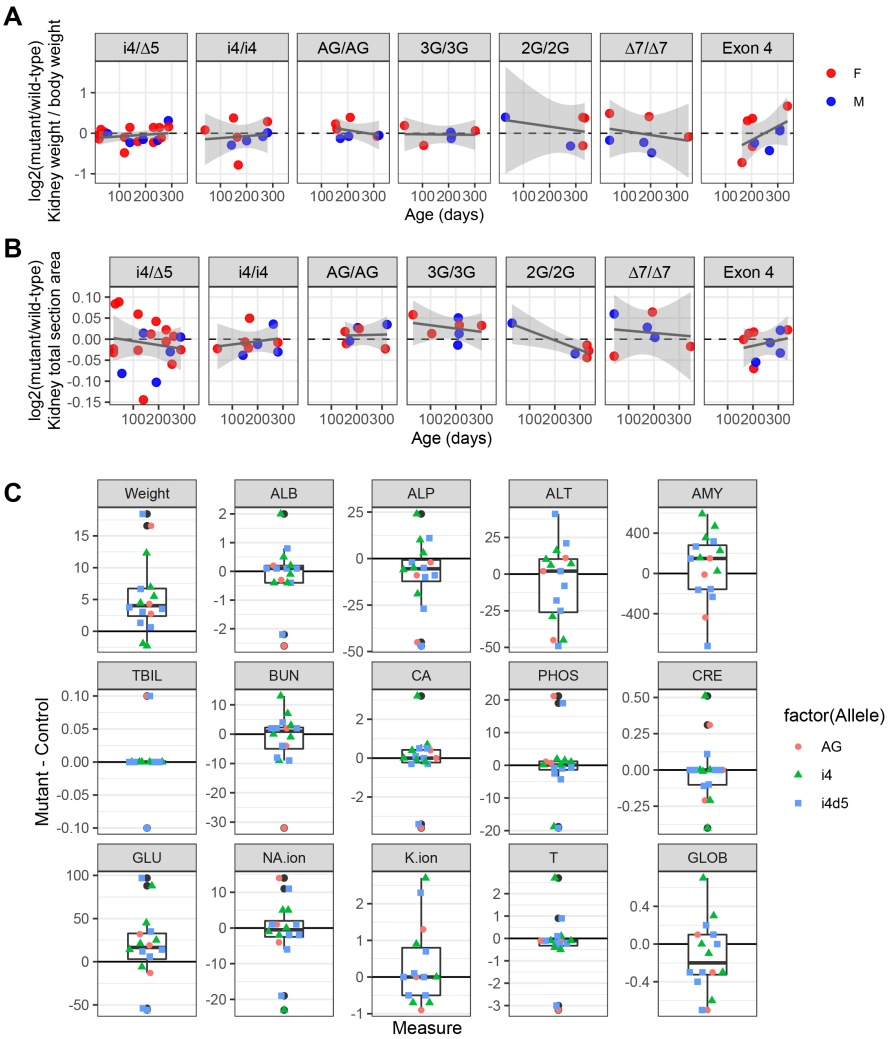

Supplemental S1_Figure. Additional paired sample kidney and blood chemistry measures. (**A**) Ratio of kidney weight to body weight was not significantly different between genotypes for any variant, p >0.2. (**B**) Total cross-sectional area of kidney was not significantly different between genotypes for any variant, p >0.2. (**C**) No striking differences in blood chemistries among 16 sex-matched littermate pairs. Standard blood chemistry panels from same-sex littermate pairs from strong *Tulp3* allele combinations found no consistent differences dependent on genotype, in contrast to their body weights, which confirmed the differences shown in Figure 3.

233 This suggests that histological measures may be more sensitive than standard blood
234 chemistries for modeling ciliopathy defects in mice.
235
236 **Reduced cilium length and frequency precede cystic kidneys.**
237 We next investigated whether reduced *Tulp3* expression or exon 4 deletion affected primary
238 cilium structure and function in kidneys prior to cystogenesis, focusing on the most severe
239 viable loss of expression (i4/Δ5) and exon 4-deleted (Δ67) models compared with their sex-
240 matched littermates. We measured cilia length, frequency, and localization of TULP3 and
241 GPR161 in kidney tissue from these mice at a pre-cystic stage. We measured length of 276
242 individual cilia based on immunofluorescence for ARL13B (Figure 6A, B and S9_Table). Mean
243 cilium length was ~15% shorter in i4/Δ5 compound heterozygotes than in control littermates
244 across all four littermate pairs ($p = 6.8 \times 10^{-5}$, paired t-test) but not significantly different between
245 Δ67 homozygotes and controls ($p = 0.98$). We also measured ciliation frequency for 500-600
246 nuclei per sample (Figure 6C and S10_Table). For i4/Δ5, ciliation frequency was significant
247 decreased (OR = 0.81, $p = 3.3 \times 10^{-6}$, Fisher's exact test), while for Δ67 mutants showed a
248 modest but statistically borderline decrease (OR = 0.92, $p = 0.059$). These results suggested
249 impaired ciliogenesis, with a stronger effect in i4/Δ5.
250
251 We next examined whether cilium localization of TULP3 or its cargo protein GPR161 were
252 affected. TULP3 was infrequently localized to primary cilia in situ and neither decreased
253 expression in i4/Δ5 (OR 1.2, $p = 0.68$, Fisher's exact test) nor deletion of exon 4 (OR 0.98, p=
254 1.0) had a significant impact on TULP3 localization frequency (Figure 6D-F). GPR161 was more
255 frequently detected (Figure 6G-I) but its localization to cilia was not significantly different in
256 either i4d5 (OR = 0.99, $p = 0.95$, Fisher's exact test) or Δ67 mutants (OR = 0.99, $p = 1.0$).
257 Together, these results suggest that while ciliogenesis is impaired, residual TULP3 is properly

258 localized and able to support GPR161 trafficking and confirm that quantitative defects in

259 ciliogenesis precede cyst formation in *Tulp3* mutant kidneys.

260

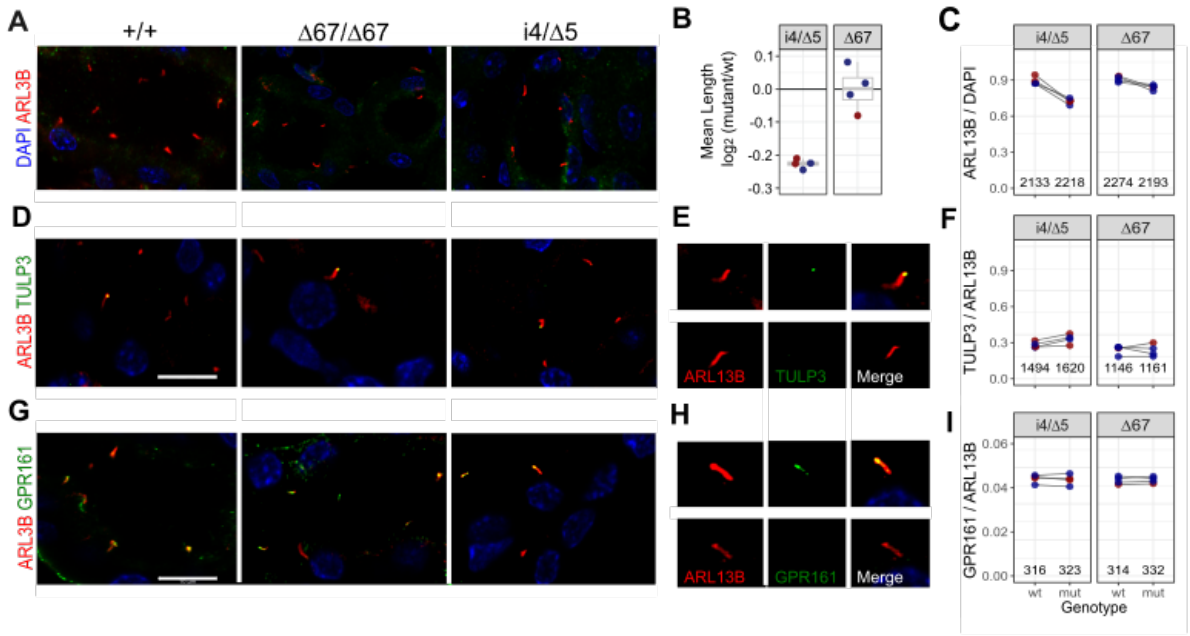

Figure 6. Hypomorphic *Tulp3* mutations affect frequency and length distribution of primary cilia. (**A**) Representative images of ARL13B immunofluorescence in primary cilia (red) with DAPI-stained nuclei (blue) from kidney sections of wild-type (+/+), i4/Δ5, and Δ67 mutant mice at postnatal day 20. Scale bar, 10 μm. (**B**) Mean cilium lengths for four littermate pairs, expressed as the $\log_2$ ratio(mutant/wild-type). Female pairs red, males blue. (**C**) Ciliation frequency quantified as the percentage of ARL13B-positive cilia from 500-600 nuclei per sample. Lines connect control (left) and *Tulp3*-mutant (right) littermate samples. (**D**) Representative images showing localization of ARL13B (red) and TULP3 (green) relative to DAPI-stained nuclei (blue). Scale bar, 10 μm. (**E**) Magnified view of a single cilium showing single channel ARL13B (red), TULP3 (green), and merged channels to show localization of TULP3 to ciliary tip (top) or not (bottom). (**F**) Low but similar frequencies of TULP3 co-localization in ARL13B-defined cilia across genotypes. Lines connect littermate pairs. (**G**)

Representative images showing ARL13B (red), GPR161 (green), and DAPI-stained nuclei (blue). Scale bar, 10 μm. (**H**) Magnified view of a single cilium showing single channel ARL13B (red), GPR161 (green), and merged channels to illustrate ciliary localization (top) or absence (bottom) of GPR161. (**I**) Quantification of GPR161 localization to cilia, expressed as the percentage of GPR161-positive cilia with ARL13B signal. Lines connect littermate pairs.

261

262 ***Tulp3* reduction does not suppress major *Zfp423* brain phenotypes.**

263 We previously showed that *TULP3/Tulp3* is a repressive target of the ZNF423 (mouse ZFP423)
264 transcription factor in both mouse granule cell progenitors and a human medulloblastoma
265 (DAOY) cell line and that simultaneous knockdown of both genes reversed a SMO translocation
266 defect of *ZNF423* knockdown in DAOY cells [14]. To test whether germline mutations that
267 decrease *Tulp3* level suppress *Zfp423* developmental phenotypes at an anatomical level, we
268 crossed *Zfp423* null as well as two ZFP423 domain-specific mutations to the *Tulp3*-i4/Δ5
269 combination, in a coisogenic FVB/NJ background and measured weight and eight
270 neuroanatomical parameters that we previously used to quantify a *Zfp423* allelic series [26]
271 (Figure 7).

272

273 We first compared *Zfp423*-null mutants (N515Tfs*43, also known as N507Tfs*43 or
274 *Zfp423*^{em5Haml}) with or without strongly reduced *Tulp3* expression (Figure 7A and S11_Table).
275 Because *Zfp423* null homozygotes have reduced viability, we compared sex-matched mutant-
276 wildtype pairs between two crosses of *Zfp423* heterozygotes, one in which all animals were
277 *Tulp3* wild-type and one in which parents were *Tulp3*-i4/Δ5, resulting in offspring that were
278 either i4/Δ5 or i4/i4. In the latter cross, paired samples had the same *Tulp3* genotype. We then
279 compared the means of pair-wise differences between the two crosses. While seven out of nine
280 measures trended toward improvement in the double mutant, neither individual measures nor

281 the overall trend met even nominal significance at conventional statistical thresholds. While
282 these results did not rule out a minor effect of *Tulp3* on *Zfp423* null phenotypes, nor an effect on
283 some cell-level phenotype, they did not support the hypothesized genetic suppressor activity at
284 the level of *Zfp423* brain structural abnormalities.
285
286 We also examined the effect of *Tulp3* on two viable and fertile alleles of *Zfp423* (Figure 7B and
287 S12_Table). *Zfp423* encodes 30 C2H2 zinc finger domains and an additional putative non-
288 canonical 4-cysteine zinc finger [28], clusters of which mediate several known physical
289 interactions [22, 29-32], including a C-terminal homophilic interaction domain and SMAD
290 protein-interacting region in zinc fingers 14-19. Both a 210-bp in-frame deletion (Δ210) that
291 eliminated the 4-cysteine zinc finger region in the homophilic interaction domain and a 261-bp
292 deletion (Δ261) that fused the first half of zinc fingers 15 to the second half of zinc finger 18 in
293 the SMAD-interacting region resulted in quantifiable defects in weight and brain measures [26].
294 We used crosses in which both parents were homozygous for one of these two *Zfp423* domain

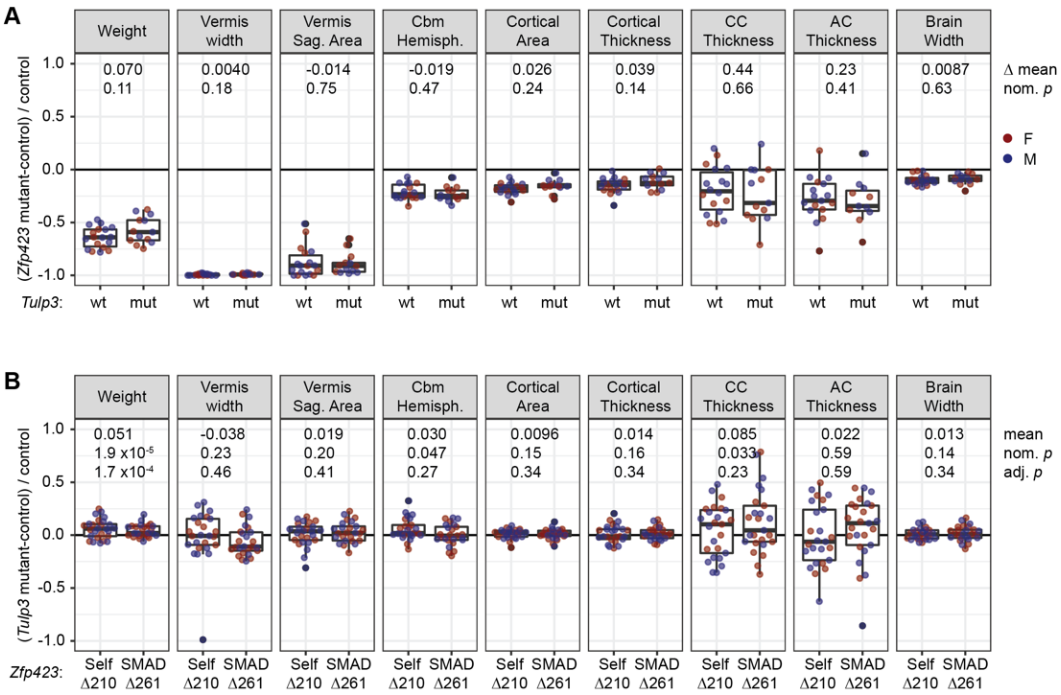

Figure 7. Genetic reduction of *Tulp3* does not suppress *Zfp423* null or hypomorphic phenotypes. (**A**) Major *Zfp423*-null phenotypes are not substantially improved by reduced *Tulp3* expression. Each point represents a *Zfp423* mutant-wildtype same-sex littermate pair, from crosses with *Zfp423*^{N507Tfs*43} heterozygous and either *Tulp3* wild-type (wt, n=18), or *Tulp3* i4/Δ5 (mut, n=13) parents. Differences in the means between *Zfp423* and double mutants along with nominal *p*-values from Welch Two Sample t-test are given. (**B**) *Tulp3* reduction had only nominal effects on *Zfp423* hypomorph measures other than weight. Homozygotes for viable in-frame deletions of a self-association domain (Δ210) or SMAD-binding zinc fingers (Δ261) with viable reductions in *Tulp3* (i4/Δ5 or i4/i4) were compared to same-sex littermates homozygous for the same *Zfp423* mutation but wild-type for *Tulp3*. Self-association domain n=26 pairs, SMAD-binding domain n=25 pairs. Paired sample t-tests or Wilcoxon signed rank test (vermis width) before and after adjustment for family-wise error rate (Hommel's method) are shown for the combined sample (n=51). Effects on weight were independently significant in each group.

295 deletions and heterozygous for *Tulp3*-i4 in one parent and *Tulp3*-Δ5 in the other to produce
296 same-sex littermate pairs of *Zfp423* hypomorphs that are *Tulp3* wild-type or i4/Δ5. We observed
297 nominal improvements in weight, anterior-posterior distance in cerebellar hemispheres, and
298 thickness of the corpus callosum, but each effect had small magnitude and only weight survived
299 correction for family-wise error rate across the nine measures. These results suggest that *Tulp3*
300 reduction may have had a suppressing effect on some *Zfp423* anatomical phenotypes in
301 hypomorphic variants, but that any effect sizes were quite small relative to the *Zfp423* main
302 effects.

303

304 **DISCUSSION**

305 Here we demonstrated a simple method for creating a quantitative allelic series in mice and
306 identified distinct TULP3 levels required for viability, neuroanatomical measures, kidney
307 homeostasis, and obesity and used that series to calibrate a qualitative allele affecting both
308 expression level and protein composition. These results provide a generalizable strategy for
309 efficient quantitative animal models of genetic disorders and identify new features of *Tulp3*
310 pathology in mice.

311

312 From a single "one-pot" CRISPR/Cas9 editing experiment at exon 7, we recovered 6
313 functionally distinct alleles (counting only one of two presumptive nulls, Figure 1) targeting the
314 polypyrimidine tract adjacent to an essential, frame-shifting exon. Null variants recapitulated
315 expected embryonic lethal phenotypes, including polydactyly and exencephaly, while other
316 recovered alleles that reduced *Tulp3* RNA and protein expression showed a range of
317 phenotypes that correlated with reduction in expression level. Our approach should be
318 extensible to other genes, though details may vary with the strength of cis-acting signals for
319 exon inclusion. This approach allows more accurate modeling of pathogenic variants by
320 calibrating the amount of genetic function required for measured phenotypes with much more
321 precision than simple null and heterozygote collections in large-scale phenotyping centers.

322

323 Our results support different quantitative requirements for TULP3 among affected tissues.
324 Measures across calibrated *Tulp3* genotypes allowed us to assess quantitative thresholds and
325 dose-responses for several notable phenotypes (Figure 8). The data showed a low threshold
326 (~5% of control) to allow viability while avoiding polydactyly and severe neural tube defects,
327 although the strongest viable genotype had measurable if slight increases in some
328 morphological brain measures. Among viable genotypes, we found significant excess weight
329 relative to littermates that expressed less than one-third of control TULP3 levels, with a slightly

330 larger impact of exon 4 deletion relative to its measured expression level. Obesity is a cardinal
331 feature of mutations in *Tub*, the close paralog of *Tulp3* and eponymous founding member of the
332 gene family [33-36]. Whether and to what extent variants at either locus might modify
333 phenotypic expression of the other remains to be tested. Notably, we found later onset and less
334 severe kidney phenotypes for viable *Tulp3* variant combinations in our FVB-coisogenic models
335 than previous reports from mice on C57BL/6 or mixed backgrounds, despite inclusion of very
336 strong reductions in TULP3 expression level. These differences may include effects of genetic
337 modifiers, but we note that presumptive null variants on FVB recapitulate prior phenotypes. This
338 suggests that substitution variants with highly cystic kidneys by birth, such as K407I [37],
339 represent severe loss of function. Further studies will be required to determine whether these
340 differences indicate strain-dependent genetic modifiers or environmental differences. Our data
341 also showed that kidney cystogenesis had a quantitative dose-response to TULP3 level across
342 a range from ~5-30% of control levels. Notably, this is a range that is not addressed in large
343 consortia that assess knockout and heterozygote models. Prior to detectable cystogenesis,
344 kidneys showed a decrease in the frequency of primary cilia and in length of observed cilia, at
345 least in the strongest viable genotype, i4/Δ5, but we did not find a significant difference in the
346 proportion of evident cilia that were stained for either TULP3 or GPR161. We also found no
347 evidence for *Tulp3*-mediated suppression of *Zfp423* phenotypes predicted from cell culture
348 assays. This highlights the importance of in situ validation of acute perturbation cell culture
349 models of complex tissue-level phenotypes. These data provide a unique quantitative
350 framework for modeling human *TULP3* effects in mice with a generalizable approach and for
351 estimating quantitative effects of qualitative protein variants.
352

	Δ5/Δ5	i4/Δ5	i4/i4	AG/AG	3G/3G	exon 4	Δ7/Δ7	2G/2G
Protein expression	0.03 ±.03	0.06 ±.02	0.08 ±.02	0.06 ±.02	0.08 ±.05	0.25 ±.10	0.36 ±.05	0.67 ±.03
Lethality	100	0	0	0	0	0	0	0
Polydactyly	100	0	0	0	0	0	0	0
Brain morphology	Severe	Slight	0	0	0	0	0	0
Weight excess	nd	4.5 g	1.5 g	1.5 g	1.5 g	1.8 g	ns	ns
Kidney cysts	(Severe)	2.8	1.8	1.7	0.72	0.29	0.02	0.14

Figure 8. Summary of TULP3 expression-dependent effects. Heat map shows mean protein level in E14.5 embryo heads (top row, blue) inversely proportional to measured phenotypes (rows 2-6, red). Very low levels of TULP3 expression are sufficient to avoid lethality and polydactyly. Only the lowest viable expression level has residual brain morphological abnormalities relative to same-sex control littermates. Genotypes with less than ~36% TULP3 expression show increased weight gain, with average values relative to same-sex littermates at ~100 days shown. Cystic index in kidneys showed continuous graded response to TULP3; interpolated average at 200 days is shown; severity of the null inferred from embryonic and juvenile kidneys of earlier *Tulp3* models [16, 17]. nd, not determined; ns, no significant difference.

353

354 **MATERIALS AND METHODS**

355

356 **Mice.** FVB/NJ mice were purchased from The Jackson Laboratory. *Zfp423* mutant mice were
357 previously reported [26] and maintained coisogenic on FVB/NJ. Mice were maintained in a
358 specific pathogen free (SPF) facility on 12 h light, 12 h dark cycle in high-density racks with
359 HEPA-filtered air and ad libitum access to water and food (LabDiet 5P06). All animal
360 experiments were approved by the University of California San Diego Institutional Animal Care
361 and Use Committee (UCSD-IACUC) under protocol S00219.

362

363 **Germline editing.** Genome editing was contemporaneous with and essentially as described by
364 Deshpande et al. [26]. Briefly, FVB/NJ one-cell embryos were injected with pre-assembled
365 editing mixes in IDTE (10 mM Tris, 0.1 mM EDTA, pH 8.0) and transplanted into pseudo-
366 pregnant females in the UC San Diego Moores Cancer Center Transgenic Mouse Shared
367 Resource facility. Editing mixes were formulated by annealing tracrRNA and crRNA for ~30
368 minutes in IDTE or 0.5x duplex buffer (0.5x is 15 mM HEPES, pH 7.5; 50 mM potassium
369 acetate), incubating with diluted Cas9 for 5 minutes (exon 4) or HiFi Cas9 for 15 minutes (exon
370 7), diluting the resulting complex in IDTE, and supplementing with oligonucleotide pools
371 (Ultramers) as donors for homology-dependent repair. Diluted editing mixes as injected
372 contained 1.2 to 1.5 μM crRNA:tracrRNA, 30 ng/μl Cas9 or HiFi Cas9, and 2.4 to 3.2 μM pooled
373 Ultramer oligonucleotides. Targeting sequences for each crRNA, with protospacer-adjacent
374 motif (PAM, in parentheses), were: CAGCTGGACCGTCGATGCCT (AGG) and
375 TAGGAGCACATCCCCGCAAC (CGG) for exon 4 and CCGGCTAGAAGAAATATCTG (AGG)
376 for exon 7. Ultramer oligonucleotide sequences are given in Supplemental Table S1. All editing
377 components were purchased from Integrated DNA Technologies (IDT). Tail biopsy DNAs from
378 potential founder (G0) animals were used for PCR-based sequencing using primers in
379 Supplemental Table S2. Edited lines were maintained coisogenic by serial backcross to

380 FVB/NJ. Genotypes for stock maintenance and experimental subjects were determined by PCR
381 assays (Supplemental Table S2). Nucleotide substitution allele (2G, 3G, and AG) used
382 bidirectional-PCR amplification of specific alleles (biPASA) assay designs [38] unique to each
383 allele.
384
385 **RT-PCR.** RNA was extracted with Trizol reagent from E14.5 embryo heads and reverse
386 transcribed with SuperScriptIII (Invitrogen). Exon inclusion assays used 35 cycles of PCR with
387 primers in flanking exons (Supplemental Table S2) and resulting products resolved by gel
388 electrophoresis.
389
390 **Western blots.** Staged embryos were obtained by timed mating after 5 pm, with noon of the
391 following day designated E0.5. Protein extracts from E14.5 heads were prepared in RIPA buffer
392 (Teknova, R3792) supplemented with protease inhibitors (Sigma-Aldrich, P8340) from mutant
393 and control littermate samples were separated in 13% acrylamide gels and electrophoretically
394 transferred to nitrocellulose membranes (GVS, 1212590). After blocking in 5% non-fat dry milk
395 (APEX, 20-241), membranes were exposed to rabbit anti-TULP3 ([2], gift of Dr. Jonathan
396 Eggenschwiler) anti-phosphoprotein antibodies as a loading control (MilliporeSigma, P3300,
397 P3430, P3555) followed by IR-680 conjugated donkey anti-mouse (LiCOR 926-68072) and IR-
398 800 conjugated donkey anti-rabbit (LiCOR 926-32213) secondary antibodies. After washing 3x
399 in TBST (20 mM Tris, 150 mM NaCl, 0.1% Triton X-100) retained antibodies were imaged on a
400 LI-COR Odyssey imaging station and bands quantified using ImageStudio software (LiCOR).
401
402 **Anatomical measures.** Sequential, paired samples were weighed ~weekly for up 300 days. A
403 small number of animals, predominantly females, developed circling behavior independent of
404 genotype and were removed from the study. Simple brain morphological measures were made
405 as described for *Zfp423* mutants [26]. Briefly, anesthetized mice were perfused with phosphate

406 buffer followed by 4% paraformaldehyde. Brains were removed and post-fixed in 4%
407 paraformaldehyde at 4°C overnight. External dorsal and block face coronal and sagittal images
408 were captured on a Zeiss stereoscope with a Nikon Ds-Fi1 camera and measurements made in
409 ImageJ software [39]. Kidneys were post-fixed in 4% paraformaldehyde overnight, then
410 cryoprotected in 20% sucrose, 1X PBS, 0.5 mM EDTA. Tissues were embedded in O.C.T.
411 compound (Fisher Scientific, 23-730-571) and flash frozen using 2-methylbutane cooled on dry
412 ice. 15 µm sections were cut using a Leica CM3050S Cryostat at -20°C. After staining with
413 hematoxylin and eosin, sections were photographed and cystic index was measured using
414 CystAnalyzer software [27] using a 10 µm diameter setting.
415
416 **Cilium measures.** Kidneys were prepared from sex-matched littermate pairs as above at
417 postnatal day 20. 10 µm sections were cut at −20°C. Sections were washed in PBS three times
418 for 5 minutes each and permeabilized with 0.1% Triton X-100 in PBS for 10 minutes. Sections
419 were blocked with 5% donkey serum, 1% bovine serum albumin (BSA), and 0.1% Triton X-100
420 in PBS for 60 minutes at room temperature. Slides were incubated overnight at 4 °C with
421 primary antibodies diluted in blocking buffer. Mouse anti-γ-tubulin (Sigma, T5326) and rabbit
422 anti-ARL13B (Proteintech, 17711-1-AP) were used to measure cilia length. Mouse anti-ARL13B
423 (Santa Cruz Biotechnology, sc-515784), rabbit anti-TULP3 (Proteintech, 13637-1-AP), and
424 rabbit anti-GPR161 (Proteintech, 29328-1-AP) were used to assess the localization of TULP3
425 and GPR161. Sections were washed three times with PBS the following day and incubated with
426 fluorophore-conjugated secondary antibodies (Invitrogen, A21203 and A21206) for 1 hour at
427 room temperature in the dark. After three additional PBS washes, nuclei were stained with DAPI
428 for 3 minutes, followed by a brief PBS rinse. Slides were mounted with Cytoseal 60 (Electron
429 Microscopy Sciences, 18006), cover slipped and sealed. Fluorescence images were acquired at
430 the UCSD Microscopy Core using a Leica SP8 confocal microscope equipped with Lightning
431 Deconvolution. Image analysis was performed using LASX software on 5 µm Z-stack images.

Statistical analyses. Data were visualized using ggplot2 with the ggbeeswarm package [40]. Data were assessed for normality using the Shapiro-Wilk test and evaluated for differences between same-sex littermates of opposite genotype using either parametric (t-test) or nonparametric (Wilcoxon signed rank test) for paired samples. Resulting nominal p-values were corrected for family-wise error rate (FWER) across phenotypes using Hommel's method [25]. Survival analysis was performed using a Cox proportional hazards model in the survival package. All statistical tests were performed in R.

Ethics statement

All animal experiments were approved by the University of California San Diego Institutional Animal Care and Use Committee (UCSD-IACUC) under protocol S00291.

ACKNOWLEDGEMENTS

We thank Dr. Jonathan Eggenschwiler for the gift of TULP3 antibody. We thank Ella Kothari and Jun Zhao for mouse zygote injections performed in the UCSD Moores Cancer Center Transgenic Mouse Core Facility. We thank Oliver Zhang for genotyping assistance and reading the draft manuscript.This work was supported by grant R01 NS097534 from the National Institute of Neurological Disorders and Stroke to BAH. CAM was supported in part by a training grant from the National Cancer Institute, T32 CA067754. RZL was supported in part by an institutional grant from the National Institute of General Medical Sciences, R25 GM083275. The UC San Diego Transgenic Mouse Core is supported by NIH P30 CA023100 and P30 DK063491. The UC San Diego School of Medicine Microscopy Core is supported by P30 NS047101. The funders had no role in study design, data collection and analysis, decision to publish, or preparation of the manuscript.

DATA AVAILABILITY

All graphical summary plots show individual measures as dots. Underlying tabular data are in supporting tables formatted as data frames.

COMPETING INTERESTS

The authors have declared that no competing interests exist.

466 **REFERENCES**

467 1. Santagata, S., et al., *G-protein signaling through tubby proteins.* Science, 2001.
468 **292**(5524): p. 2041-50.
469 2. Norman, R.X., et al., *Tubby-like protein 3 (TULP3) regulates patterning in the mouse*
470 *embryo through inhibition of Hedgehog signaling.* Hum Mol Genet, 2009. **18**(10): p.
471 1740-54.
472 3. Nishina, P.M., et al., *Molecular characterization of a novel tubby gene family member,*
473 *TULP3, in mouse and humans.* Genomics, 1998. **54**(2): p. 215-20.
474 4. Mukhopadhyay, S., et al., *TULP3 bridges the IFT-A complex and membrane*
475 *phosphoinositides to promote trafficking of G protein-coupled receptors into primary cilia.*
476 Genes Dev, 2010. **24**(19): p. 2180-93.
477 5. Mukhopadhyay, S., et al., *The ciliary G-protein-coupled receptor Gpr161 negatively*
478 *regulates the Sonic hedgehog pathway via cAMP signaling.* Cell, 2013. **152**(1-2): p. 210-
479 23.
480 6. Chávez, M., et al., *Modulation of Ciliary Phosphoinositide Content Regulates Trafficking*
481 *and Sonic Hedgehog Signaling Output.* Dev Cell, 2015. **34**(3): p. 338-50.
482 7. Garcia-Gonzalo, F.R., et al., *Phosphoinositides Regulate Ciliary Protein Trafficking to*
483 *Modulate Hedgehog Signaling.* Dev Cell, 2015. **34**(4): p. 400-409.
484 8. Badgandi, H.B., et al., *Tubby family proteins are adapters for ciliary trafficking of integral*
485 *membrane proteins.* J Cell Biol, 2017. **216**(3): p. 743-760.
486 9. Palicharla, V.R., et al., *Interactions between TULP3 tubby domain and ARL13B*
487 *amphipathic helix promote lipidated protein transport to cilia.* Mol Biol Cell, 2023. **34**(3):
488 p. ar18.
489 10. Palicharla, V.R., et al., *A defined tubby domain beta-barrel surface region of TULP3*
490 *mediates ciliary trafficking of diverse cargoes.* Mol Biol Cell, 2025. **36**(1): p. ar1.

491 11. Cameron, D.A., T. Pennimpede, and M. Petkovich, *Tulp3 is a critical repressor of mouse*
492 *hedgehog signaling.* Dev Dyn, 2009. **238**(5): p. 1140-9.
493 12. Patterson, V.L., et al., *Mouse hitchhiker mutants have spina bifida, dorso-ventral*
494 *patterning defects and polydactyly: identification of Tulp3 as a novel negative regulator*
495 *of the Sonic hedgehog pathway.* Hum Mol Genet, 2009. **18**(10): p. 1719-39.
496 13. Mukhopadhyay, S. and P.K. Jackson, *The tubby family proteins.* Genome Biol, 2011.
497 **12**(6): p. 225.
498 14. Hong, C.J. and B.A. Hamilton, *Zfp423 Regulates Sonic Hedgehog Signaling via Primary*
499 *Cilium Function.* PLoS Genet, 2016. **12**(10): p. e1006357.
500 15. Ikeda, A., et al., *Neural tube defects and neuroepithelial cell death in Tulp3 knockout*
501 *mice.* Hum Mol Genet, 2001. **10**(12): p. 1325-34.
502 16. Hwang, S.H., et al., *Tulp3 Regulates Renal Cystogenesis by Trafficking of Cystoproteins*
503 *to Cilia.* Curr Biol, 2019. **29**(5): p. 790-802.e5.
504 17. Legué, E. and K.F. Liem, Jr., *Tulp3 Is a Ciliary Trafficking Gene that Regulates*
505 *Polycystic Kidney Disease.* Curr Biol, 2019. **29**(5): p. 803-812.e5.
506 18. Devane, J., et al., *Progressive liver, kidney, and heart degeneration in children and*
507 *adults affected by TULP3 mutations.* Am J Hum Genet, 2022. **109**(5): p. 928-943.
508 19. Shaheen, R., et al., *POC1A truncation mutation causes a ciliopathy in humans*
509 *characterized by primordial dwarfism.* Am J Hum Genet, 2012. **91**(2): p. 330-6.
510 20. Garaycoechea, J.I., C. Quinlan, and M.S. Luijsterburg, *Pathological consequences of*
511 *DNA damage in the kidney.* Nat Rev Nephrol, 2023. **19**(4): p. 229-243.
512 21. Choi, H.J., et al., *NEK8 links the ATR-regulated replication stress response and S phase*
513 *CDK activity to renal ciliopathies.* Mol Cell, 2013. **51**(4): p. 423-39.
514 22. Chaki, M., et al., *Exome capture reveals ZNF423 and CEP164 mutations, linking renal*
515 *ciliopathies to DNA damage response signaling.* Cell, 2012. **150**(3): p. 533-48.

516 23. Airik, R., et al., *Renal-retinal ciliopathy gene Sdccag8 regulates DNA damage response*
517 *signaling.* J Am Soc Nephrol, 2014. **25**(11): p. 2573-83.
518 24. Qu, Q., et al., *Lithocholic acid binds TULP3 to activate sirtuins and AMPK to slow down*
519 *ageing.* Nature, 2024.
520 25. Hommel, G., *A stagewise rejective multiple test procedure based on a modified*
521 *Bonferroni test.* Biometrika, 1988. **75**(2): p. 383-386.
522 26. Deshpande, O., et al., *ZNF423 patient variants, truncations, and in-frame deletions in*
523 *mice define an allele-dependent range of midline brain abnormalities.* PLoS Genet,
524 2020. **16**(9): p. e1009017.
525 27. Cordido, A., et al., *CystAnalyser: A new software tool for the automatic detection and*
526 *quantification of cysts in Polycystic Kidney and Liver Disease, and other cystic disorders.*
527 PLoS Comput Biol, 2020. **16**(10): p. e1008337.
528 28. Hamilton, B.A., *ZNF423 orthologs are highly constrained in vertebrates but show*
529 *domain-level plasticity across invertebrate lineages.* bioRxiv, 2020: p.
530 2020.03.09.984518.
531 29. Tsai, R.Y. and R.R. Reed, *Cloning and functional characterization of Roaz, a zinc finger*
532 *protein that interacts with O/E-1 to regulate gene expression: implications for olfactory*
533 *neuronal development.* J Neurosci, 1997. **17**(11): p. 4159-69.
534 30. Tsai, R.Y. and R.R. Reed, *Identification of DNA recognition sequences and protein*
535 *interaction domains of the multiple-Zn-finger protein Roaz.* Mol Cell Biol, 1998. **18**(11): p.
536 6447-56.
537 31. Hata, A., et al., *OAZ uses distinct DNA- and protein-binding zinc fingers in separate*
538 *BMP-Smad and Olf signaling pathways.* Cell, 2000. **100**(2): p. 229-40.
539 32. Lauberth, S.M. and M. Rauchman, *A conserved 12-amino acid motif in Sall1 recruits the*
540 *nucleosome remodeling and deacetylase corepressor complex.* J Biol Chem, 2006.
541 **281**(33): p. 23922-31.

542 33. Coleman, D.L. and E.M. Eicher, *Fat (fat) and tubby (tub): two autosomal recessive*
543 *mutations causing obesity syndromes in the mouse.* J Hered, 1990. **81**(6): p. 424-7.
544 34. Kleyn, P.W., et al., *Identification and characterization of the mouse obesity gene tubby: a*
545 *member of a novel gene family.* Cell, 1996. **85**(2): p. 281-90.
546 35. Noben-Trauth, K., et al., *A candidate gene for the mouse mutation tubby.* Nature, 1996.
547 **380**(6574): p. 534-8.
548 36. North, M.A., et al., *Molecular characterization of TUB, TULP1, and TULP2, members of*
549 *the novel tubby gene family and their possible relation to ocular diseases.* Proc Natl
550 Acad Sci U S A, 1997. **94**(7): p. 3128-33.
551 37. Legué, E. and K.F. Liem, Jr., *Mutations in Ciliary Trafficking Genes affect Sonic*
552 *Hedgehog-dependent Neural Tube Patterning Differentially along the Anterior-Posterior*
553 *Axis.* Neuroscience, 2020. **450**: p. 3-14.
554 38. Liu, Q., et al., *Overlapping PCR for bidirectional PCR amplification of specific alleles: a*
555 *rapid one-tube method for simultaneously differentiating homozygotes and*
556 *heterozygotes.* Genome Res, 1997. **7**(4): p. 389-98.
557 39. Schneider, C.A., W.S. Rasband, and K.W. Eliceiri, *NIH Image to ImageJ: 25 years of*
558 *image analysis.* Nat Methods, 2012. **9**(7): p. 671-5.
559 40. Wickham, H., *ggplot2: Elegant Graphics for Data Analysis*. 2016, New York: Springer-
560 Verlag.
561
562

563 **Supporting Information captions**

564 **S1_Table. Sequence of oligonucleotide donors used in editing exon 7.** Oligonucleotide
565 donors used for genome editing in Figure 1C. The guide RNA sequences are given in the
566 Materials and Methods.

567

568 **S2_Table. PCR primers used for screening and genotyping.** Left and right primers used to
569 sequence potential founders and transmitted alleles for *Tulp3* exon 4 and exon 7 shown in
570 Figure 1. The same exon 4 primers were used to genotype deletion alleles. Genotyping primers
571 for biPASA assays included common "outer" primers with allele-specific inner primers for the
572 reference (wt) and substituted (2G, 3G, or AG) allele. Short indel variants at exon 7 were typed
573 using a 74-bp assay (Tx7.74). Exon 7 RT-PCR inclusion assay used a forward primer in exon 6
574 and reverse primer in exon 8.

575

576 **S3_Table. Normalized fluorescence values from Western blots.** Measures used in Figure
577 1H. Animal ID, genotype, and expression values from Western blots of extracts from embryonic
578 day (E)14.5 samples. Mutant and heterozygote sample measures were adjusted to the intensity
579 of their wild-type control littermate (pctWT).

580

581 **S4_Table. Normalized fluorescence values from Western blots.** Measures used in Figure 1I.
582 Animal data and Western blot data for extracts from postnatal day 29 tissues. Mutant sample
583 measures were adjusted to the intensity of their wild-type control littermate.

584

585 **S5_Table. Paired sample weight measures.** Longitudinal weight measures for paired
586 littermates used to generate Figure 3. Logical variable (e.g., n75) describe whether a specific
587 measure is the first past that postnatal day for that littermate pair. Removed indicates whether a

588 measure was censored due to subsequent animal health problems for which weight change
589 may have been a leading indicator independent of genotype.
590
591 **S6_Table. Paired sample brain measures.** Terminal weight and brain measures used in
592 Figure 4. Measures follow those in Deshpande et al. [26]
593
594 **S7_Table. Paired sample kidney cystic index measures.** Animal characteristics and cystic
595 index measures used in Figure 5.
596
597 **S8_Table. Paired sample blood chemistry measures.** Terminal weight and veterinary blood
598 chemistry measures used in S1_Figure.
599
600 **S9_Table. Distribution of cilium lengths.** Length measures for 277 cilia across eight i4/Δ5
601 and Δ67 littermate pairs.
602
603 **S10_Table. Proportion of cilia with TULP3 and GPR161.** Proportions of ARL13B-stained cilia
604 that had co-localized TULP3 or GPR161 immunofluorescence.
605
606 **S11_Table. Paired sample measures from *Zfp423*-null x *Tulp3*-i4/Δ5 cross.** Terminal weight
607 and brain measures used in Figure 6A.
608
609 **S12_Table. Paired sample measures from *Zfp423*-hypomorph x *Tulp3*-i4/Δ5 cross.**
610 Terminal weight and brain measures used in Figure 6B.
611
612 **S1_Figure. Paired sample kidney and blood chemistry measures.** (**A**) Ratio of kidney
613 weight to body weight was not significantly different between genotypes for any variant, $p > 0.2$.

614 (**B**) Total cross-sectional area of kidney was not significantly different between genotypes for
615 any variant, p >0.2. (**C**) Box-and-whiskers plots with individual data points for paired sample
616 differences (mutant – littermate control) for Albumin (ALB), Alkaline Phosphatase (ALP), Alanine
617 Transaminase (ALT), Amylase (AMY), total Bilirubin (TBIL), Blood Urea Nitrogen (BUN),
618 Calcium (CA), Phosphorus (PHOS), Creatinine (CRE), Glucose (GLU), Sodium (NA-ion),
619 Potassium (K-ion), Total Protein (TP), and calculated Globulin (GLOB).